Communications Materials

https://doi.org/10.1038/s43246-025-01029-1

Article in Press

Photon energy-dependent ultrafast magnetization dynamics in magnetic heterostructures

Received: 28 March 2025

Accepted: 24 November 2025

Cite this article as: Yu, I.C., Ko, S., Kim, W.T. *et al.* Photon energy-dependent ultrafast magnetization dynamics in magnetic heterostructures. *Commun Mater* (2025). https://doi.org/10.1038/s43246-025-01029-1

In Cheol Yu, San Ko, Won Tae Kim, Byong-Guk Park, Byoung S. Ham, Kab-Jin Kim & Fabian Rotermund

Photon Energy-Dependent Ultrafast Magnetization Dynamics in Magnetic Heterostructures

In Cheol Yu[1†], San Ko[1†], Won Tae Kim[1], Byong-Guk Park[2], Byoung S. Ham[3], Kab-Jin Kim[1*], and Fabian Rotermund[1*]

[1]*Department of Physics, Korea Advanced Institute of Science and Technology (KAIST), Daejeon 34141, Republic of Korea*

[2]*Department of Materials Science and Engineering, Korea Advanced Institute of Science and Technology (KAIST), Daejeon 34141, Republic of Korea*

[3]*School of Electrical Engineering and Computer Science, GIST, Gwangju 61005, Republic of Korea*

[†]These authors contributed equally to this work

*Corresponding authors: rotermund@kaist.ac.kr (F.R.); kabjin@kaist.ac.kr (K.-J.K.)

Abstract

Laser-induced ultrafast demagnetization has traditionally been understood as a process in which photon absorption excites nonequilibrium electrons, leading to demagnetization followed by magnetization recovery. It has been widely assumed that the time scale of these dynamics is governed primarily by the total absorbed laser power rather than the specific photon energy. In this study, we challenge this assumption by employing spintronic terahertz emission spectroscopy, a technique primarily sensitive to spin transport rather than local magnetization changes. We reveal that the time scales of both demagnetization and recovery systematically vary with laser wavelength. Specifically, magnetization dynamics induced by shorter-wavelength optical pulses evolve over significantly longer time scales than those triggered by longer-wavelength infrared pulses, even at constant absorbed power. Our findings suggest that higher-energy (shorter-wavelength) photons enhance magnon excitation, which drives spin transport across the magnet/nonmagnet interface, thereby modifying the magnetization dynamics. These results highlight the direct influence of photon energy on ultrafast demagnetization, building upon and complementing earlier studies from various perspectives, while also offering new opportunities for optical control of spintronic phenomena.

Introduction

Spintronic research demands ever-faster control of spin angular momentum to facilitate efficient spin state manipulation, collective magnetic excitations, and spin current generation. A promising approach to achieving ultrafast spin control is laser-induced spin manipulation. In this process, intense optical pulses generate nonequilibrium electrons, which subsequently relax through electron-phonon scattering. As they transfer angular momentum to the lattice, the spin polarization undergoes an ultrafast reduction—a phenomenon known as ultrafast demagnetization [1,2].

Despite extensive investigations over the past two decades [3-17], the mechanisms underlying ultrafast demagnetization remain controversial. The magnetic response to a laser pulse is intrinsically linked to electronic dynamics, either through direct excitation by the laser field or via secondary scattering processes. Traditionally, most studies have attributed demagnetization to the latter [18], emphasizing that the laser primarily acts as an ultrafast heating source [1-6,19]. However, a growing experimental evidence suggests that direct optical excitation plays a significant role in ultrafast demagnetization [11,20-23]. This implies that the shape of the optically excited electronic distribution may be a key factor in governing demagnetization dynamics.

When electrons absorb photons, they gain energy and transition to unoccupied states above the Fermi level, leading to a deviation from the Fermi-Dirac distribution. The shape of this nonequilibrium electron distribution is primarily determined by the photon energy of the laser, which is directly related to its wavelength. Consequently, if demagnetization is significantly influenced by the initial nonequilibrium electron distribution [24-26], the resulting spin dynamics should vary depending on the laser wavelength. Conversely, if demagnetization is driven purely by a thermal process [1,2,5,19], the spin dynamics should remain unchanged as long as the total absorbed power is constant, regardless of the laser wavelength.

Previous studies have reported conflicting results regarding the influence of laser wavelength on ultrafast demagnetization. Magneto-optical experiments on Fe/glass and Ni/MgO suggested that demagnetization depends solely on the total absorbed power and is independent of the laser wavelength [27,28]. In contrast, studies on Ni/Au and Co/Pt bilayers found that demagnetization is significantly affected by the laser wavelength, with spin dynamics induced by 400-nm pump pulses

evolving more slowly than those triggered by near-infrared pump pulses [18,29,30]. However, these studies attributed the observed wavelength-dependent dynamics to variations in absorbed laser fluence, suggesting that the 400-nm laser is simply absorbed more efficiently. As a result, they still support the conventional view that demagnetization is governed by total absorbed laser power rather than the specific laser wavelength.

In this work, we present evidence that challenges the conventional understanding of ultrafast spin dynamics. We investigated the demagnetization process in magnet/nonmagnet heterostructures using spintronic terahertz (THz) emission spectroscopy, where changes in magnetization are directly reflected in the THz field amplitude [31,32]. To analyze the demagnetization process unambiguously, we employed double-pump THz emission spectroscopy, using two laser pulses of different wavelengths—one to induce magnetization dynamics and the other to probe them via THz emission. By carefully controlling the absorbed electronic energy across different wavelengths, we observed that the demagnetization induced by shorter-wavelength pump pulses evolves significantly more slowly than that induced by longer-wavelength pump pulses. This result indicates that spin dynamics during demagnetization are strongly influenced by laser wavelength, challenging the conventional assumption that total absorbed power is the primary governing factor.

Results

THz emission via inverse spin Hall effect

Figure 1a presents a schematic of spintronic THz emission in a magnet/nonmagnet bilayer. 150-fs laser pulses are injected into the magnetic layer, where the magnetic moment is initially aligned along the *x*-direction, M^x. This excitation generates a spin current, j_s^z, flowing from the magnet into the nonmagnet. In the nonmagnet layer, this spin current is converted into a charge current via the inverse spin Hall effect (ISHE) [33,34], generating a THz electric field, E_{THz}^{y} [31,35]. The resulting THz emission is detected using the electro-optic effect (see Methods and Supplementary Note 1).

For the THz measurements, we prepared two sample structures: MgO/Co (5 nm)/Pt (5 nm) and MgO/$Tb_{15}Co_{85}$ (5 nm)/Pt (5 nm). Co/Pt was chosen as a conventional ferromagnet widely used

in ultrafast demagnetization studies. The inclusion of TbCo/Pt serves two key purposes: first, it provides a control sample to examine the material dependence of ultrafast demagnetization; second, TbCo/Pt exhibits pronounced spin transport and demagnetization dynamics within the first few hundred femtoseconds, well before significant lattice heating sets in. This temporal separation makes THz spectroscopy particularly well-suited for observing spin and electron transport on femtosecond timescales [36].

We first investigate the influence of laser wavelength on the measured THz electric field. Figure 1b shows the measured E_{THz}^{y} for Co/Pt under two different pump laser wavelengths: 400 nm (blue) and 1500 nm (gray), with identical incident laser power in both cases. In both scenarios, an oscillating THz field pulse is observed, indicating that laser excitation generates a spin current pulse, which is then converted into a charge current via ISHE. The oscillation timescale of the THz pulse remains nearly identical between the two wavelengths. The same measurement for TbCo/Pt in Fig. 1c also reveals a trend consistent with that observed in Co/Pt. However, it is premature to conclude that laser wavelength has no influence on magnetization dynamics, as the THz waveform may not fully capture the complete demagnetization process, particularly the subsequent relaxation and magnetization recovery dynamics (see Supplementary Note 2).

The THz field amplitude, and thus, the laser-induced spin current strength differs between the two wavelengths. The insets in Fig. 1b and 1c show that the THz amplitude (peak-to-peak) increases with laser power. Notably, the THz amplitude curves differ slightly between wavelengths, suggesting that spin current generation depends on the laser wavelength.

Additionally, we measured the THz field amplitude while sweeping the external magnetic field. Figures 1d and 1e show the measured THz amplitude alongside the variation in magnetization recorded using a vibrating sample magnetometer (VSM). The field-dependent THz amplitude closely follows the initial magnetization of the magnetic layer and exhibits ferromagnetic hysteresis.

These results are consistent with the widely accepted understanding that the THz field is proportional to the spin current generated at the magnetic interface. This current can originate from various laser-induced processes, including ultrafast demagnetization [32], superdiffusive spin transport [15,31,37], and the spin-dependent Seebeck effect [38,39]. Although the microscopic origins of

these mechanisms differ, they all predict that the amplitude of the emitted THz field scales with both the absorbed laser energy and the initial magnetization. Therefore, the origin of the wavelength-dependent THz field amplitude observed in Figs. 1b and 1c should be related to the amount of laser power absorbed in the magnetic (Co and TbCo) layers, which can vary with the laser wavelength [30].

Previous studies have mainly attributed these absorption differences as the primary factor driving wavelength-dependent demagnetization [29,30,40]. However, in the following sections, we will demonstrate that even when the power absorbed in the magnetic layer remains constant, the demagnetization dynamics still exhibit a significant dependence on the pump wavelength.

Double-pump THz emission spectroscopy

To investigate the effect of laser wavelength on demagnetization dynamics, we employed double-pump THz emission spectroscopy (Fig. 2a). In this approach, the first pulse serves as the pump, inducing a magnetization change (ΔM), while the second pulse acts as the probe, detecting ΔM through variations in the THz field amplitude (ΔE_{THz}). By systematically varying the time delay (Δt) between the pulses, we obtain a time-resolved ΔE_{THz} curve that directly reflects the temporal evolution of ΔM. ΔE_{THz} is expected to follow ΔM in a nearly linear fashion, although small nonlinear contributions arising from higher-order spin and charge responses under strong excitation cannot be excluded. Here, the temporal resolution of $\Delta E_{\mathrm{THz}}(\Delta t)$ is limited by the optical pulse duration, rather than by the electro-optic detection bandwidth. This technique is analogous to conventional pump-probe spectroscopy, but it specifically focuses on studying spin transport across the nonmagnetic layer [41,42].

Before analyzing the demagnetization dynamics, we address potential non-magnetic effects in the double-pump method. Firstly, the pump pulse can generate its own THz field, which may interfere with the probe-induced signal. To isolate the probe-induced THz field, we employed a lock-in detection technique, modulating only the second probe pulse (see Methods for details). Second, when the pump and probe pulses overlap in time, nonlinear optical effects can induce transient sub-picosecond oscillations [43]. Following the approach outlined in Ref. 43, we eliminate these effects (see Supplementary Note 3). Third, the probe pulse itself may influence the

magnetization, thus affecting the THz signal. To verify that the observed demagnetization originates solely from the pump pulse, we measured the response by varying the probe pulse wavelength while keeping the pump wavelength fixed. The demagnetization was found to be independent of the probe wavelength, confirming that the dynamics are governed by the pump excitation (see Supplementary Note 4).

To systematically examine the wavelength dependence, we performed double-pump THz emission spectroscopy using pump pulses of different wavelengths. Figure 2b presents the ΔE_{THz} normalized by the THz amplitude E_0 at negative delays, which corresponds to ΔM in the Co/Pt bilayer, for 400 nm (blue) and 1500 nm (gray) pump pulses. Since laser absorption plays a critical role, as discussed previously, we carefully adjusted the laser fluence to ensure equivalent power absorbed in the magnetic layer. Specifically, the 400-nm pump fluence was set to F = 800 μJ/cm², while the 1500-nm pump fluence (= 900 μJ/cm^2) was tuned to yield the same THz amplitude as the 400-nm pump under single laser pulse excitation in Fig. 1b.

The results in Fig. 2b reveal distinct wavelength-dependent demagnetization behavior: demagnetization induced by the 400-nm pump occurs significantly more slowly than that induced by the 1500-nm pump. In particular, ΔE_{THz} for the 400-nm pump reaches its maximum demagnetization state at a later time compared to the 1500-nm pump (highlighted by dotted lines and arrows). Furthermore, the recovery dynamics are also slower for the 400-nm pump, indicating that both demagnetization and recovery timescales are wavelength-dependent.

Previous studies have attributed wavelength-dependent demagnetization dynamics primarily to differences in laser absorption efficiency [29,30,40]. To assess the influence of absorption, we intentionally reduced the fluence of the 400-nm pump to 0.4F, ensuring that the absorbed power of the 400-nm pump was significantly lower than that of the 1500-nm pump. The resulting demagnetization is shown as open blue symbols in Fig. 2b. As expected, at reduced fluence (0.4F), the maximum demagnetization is lower, consistent with a decrease in absorbed laser power.

To directly compare the demagnetization time scales, we normalized the data and replotted Fig. 2b as Fig. 2c. Notably, despite the significant fluence reduction, the recovery dynamics for the 400-nm pump at 0.4F remain considerably slower than those for the 1500-nm pump. This result rules out laser absorption as the primary factor driving wavelength-dependent demagnetization

dynamics, suggesting an intrinsic mechanism that governs the slower Δ*M* evolution under shorter-wavelength excitation.

To determine whether this behavior is material-specific, we conducted the same measurements on a TbCo/Pt bilayer across a range of pump wavelengths, ensuring equal absorption conditions (incident pump fluence ~ 700 μJ/cm²). Figure 3a shows that, consistent with Co/Pt, both demagnetization and recovery occur more slowly at shorter pump wavelengths. This result indicates that wavelength-dependent demagnetization dynamics are not material-specific, but rather a general phenomenon. To extract characteristic time scales, we fitted ΔE_{THz} using a function adapted from Ref. 44:

$$\left[\frac{A_1\tau_2 - A_2\tau_1}{\tau_2 - \tau_1} e^{-t/\tau_1} - \frac{\tau_2(A_1 - A_2)}{\tau_2 - \tau_1} e^{-t/\tau_2} - A_2\right] \Theta(t) * \Gamma(t). \quad (1)$$

Here, Γ(t) denotes the Gaussian pump pulse profile, * indicates convolution, and Θ(t) is the step function. The first term describes the demagnetization process with τ_1 representing the characteristic demagnetization time (τ_{Demag}). The second term accounts for recovery towards the equilibrium value ($-A_2$), with τ_2 corresponding to the characteristic recovery time (τ_{Recover}).

Figure 3b summarizes the extracted values of the τ_{Demag} and τ_{Recover}, showing that both demagnetization and recovery times decrease systematically with increasing pump wavelength.

Time-resolved magneto-optic measurement

To provide a more comprehensive understanding of wavelength-dependent magnetization dynamics, we performed additional pump-probe magneto-optical Kerr effect (MOKE) measurements on Co/Pt, TbCo/Pt, and a single MgO/Co (5 nm)/MgO (5 nm) layer. In these experiments, the first pump pulse induces Δ*M*, while a weaker, time-delayed probe pulse detects this change via polarization rotation ($\Delta\theta_{\mathrm{Kerr}}$). The 400-nm and 1500-nm pump pulses were incident normal to the sample surface, while the 800-nm probe pulse was incident at an angle of 20°. We extracted only the Kerr rotation signal defined as $\Delta\theta_{\mathrm{Kerr}}$ $[= (M_+ - M_-)/2]$, which is odd with respect to in-plane magnetization direction and correctly reflects the Δ*M* response.

Simultaneously, we measured the reflectance change ($\Delta R/R$) of the probe pulse, which captures the nonequilibrium electron distribution and subsequent lattice thermalization including

coherent phonon oscillations [25,45-47]. Because both the lattice temperature and phonon-related dynamics scale with the absorbed laser energy, the picosecond timescale $\Delta R/R$ signal provides a practical measure of the deposited energy. While we note that $\Delta R/R$ matching offers only an approximate criterion, as it does not fully account for the partitioning of energy between electrons and the lattice [25], we adopt this approach as the most feasible way under the present experimental conditions. Accordingly, we adjusted the pump fluences for the 400-nm and 1500-nm pulses such that the $\Delta R/R$ dynamics were closely matched (Fig. 4a; see Supplementary Note 5 for detailed conditions), and then acquired the corresponding $\Delta\theta_{\mathrm{Kerr}}$ data.

Figures 4b-d show the $\Delta\theta_{\mathrm{Kerr}}$ dynamics of TbCo/Pt and Co/Pt bilayers, as well as a single Co layer. Characteristic demagnetization and recovery times were extracted from $\Delta\theta_{\mathrm{Kerr}}$ by fitting with Eq. (1), and the results are summarized in Figs. 4e and 4f (bars), together with the corresponding parameters obtained from ΔE_{THz} in Figs. 2 and 3 (open circles). For the single Co layer, the extracted parameters confirm that the $\Delta\theta_{\mathrm{Kerr}}$ dynamics under 400 nm and 1500 nm excitation are equivalent within the error. In contrast, the Co/Pt and TbCo/Pt bilayers exhibit a pronounced wavelength dependence. This contrast is particularly pronounced in ΔE_{THz}, which shows wavelength dependence in both demagnetization and recovery times, whereas $\Delta\theta_{\mathrm{Kerr}}$ varies mainly in the recovery regime (Figs. 4e and 4f).

ΔE_{THz} originates from the interfacial spin-dependent potential difference and thus reflects transport-driven demagnetization processes including contributions from superdiffusive spin current, magnon-mediated spin current, and other thermally generated channels. In contrast, $\Delta\theta_{\mathrm{Kerr}}$ primarily probes the net magnetization within the optical probe volume, thereby capturing both local demagnetization and spin loss due to transport. Consequently, the demagnetization times extracted from THz emission and MOKE measurements may differ, whereas the slower recovery dynamics tend to converge, reflecting electron-phonon equilibration and spin relaxation in both the magnetic and nonmagnetic layers.

Discussion

According to established temperature models [5,6,19], ΔM is governed by the transient temperatures of electron, lattice and spin subsystems. If energy deposition alone were determining

factor, ΔM would be fully dictated by the absorbed energy, regardless of photon energy. This is consistent with our observation that the $\Delta\theta_{\mathrm{Kerr}}$ dynamics in a single Co layer are nearly identical under 400-nm and 1500-nm excitations, confirming that local demagnetization in isolated ferromagnets is primarily governed by energy deposition [19,27].

However, the magnetization dynamics in magnetic heterostructures can differ significantly. For 1500-nm excitation, the ΔM dynamics are faster compared to 400-nm excitation, implying a direct dependence of spin transport processes on the pump photon energy. These results lead to a central conclusion: the spin transport contribution, rather than the local magnetization change alone, is intrinsically dependent on the pump laser wavelength, i.e., pump photon energy (Fig. 5a).

Single-pump THz emission waveforms impose an additional constraint. Spintronic THz emission is commonly attributed to spin currents of non-thermal electrons (Fig. 5b) [15,31,32], consistent with our observation that the THz waveforms depend only weakly on pump fluence (Supplementary Note 2). Although higher-frequency components may lie outside our detection bandwidth (~2.5 THz), the invariance of THz emission with pump wavelength in Fig. 1 indicates that superdiffusive transport does not account for the observed wavelength-dependent demagnetization. Additional non-local channels are required to explain the slower demagnetization and recovery observed at shorter wavelengths.

This brings us back to the role of the initial laser-induced states and their effect on spin transport. Upon excitation, laser photons excite electrons from the valence band to unoccupied states, generating a nonequilibrium electron distribution (Fig. 5a). During its relaxation, laser-induced magnon excitations can transfer angular momentum from the localized magnetic band to the conduction electrons via electron-magnon scattering. In this picture, the rate of ΔM in the magnon bath correlates with spin current (j_s) generation (Fig. 5c) [17,48-50]. Magnon excitation is more efficient at deeper energy levels, where the asymmetry between majority and minority spin states is more pronounced. Higher-energy photons may couple more strongly to localized magnetization than lower-energy photons, thereby enhancing magnon excitation.

This mechanism influences both the subsequent demagnetization and the magnetization recovery dynamics. Due to its large spin-orbit coupling and short spin-diffusion length, the Pt layer acts as an effective spin sink, rapidly absorbing and relaxing the injected spin polarization [51]. The

ensuing recovery of the magnetization is then governed by how the hot magnon bath in the ferromagnetic layer re-equilibrates with electrons and phonons, which can occur on longer timescales than the relaxation of spin polarization near the Fermi level [52]. Within this framework, the slower remagnetization observed for shorter wavelengths directly reflects the longer cooling time of a pump-wavelength-dependent hot magnon population in the ferromagnet.

Layer-dependent absorption can also influence ΔM [30]: even under matched THz amplitude or $\Delta R/R$ conditions, the energy partition between magnetic and nonmagnetic layers may vary with wavelength, enabling wavelength-dependent thermally driven spin currents. However, such effects are typically significant only in thicker stacks [30]. In this work, each layer is 5 nm (total 10 nm), for which excitation is expected to be comparatively uniform [53], suggesting only a minor contribution under our conditions. We therefore identify magnon excitation as the dominant process underlying the wavelength-dependent ΔM.

In conclusion, our THz emission and time-resolved MOKE measurements demonstrate that information from the laser field is not entirely lost during the thermalization process but persists in the form of magnon excitations and spin current generation. Our results reveal that demagnetization dynamics are significantly slower for short-wavelength optical pulses compared to those induced by longer-wavelength infrared pulses and indicate that photon-energy-dependent nonequilibrium electron distributions play a crucial role in magnon excitation and, consequently, in shaping the demagnetization process. These findings provide a new perspective on the debated role of nonequilibrium electron distributions in ultrafast demagnetization and highlight the critical importance of angular momentum transport between the magnetic and nonmagnetic layers in determining demagnetization dynamics.

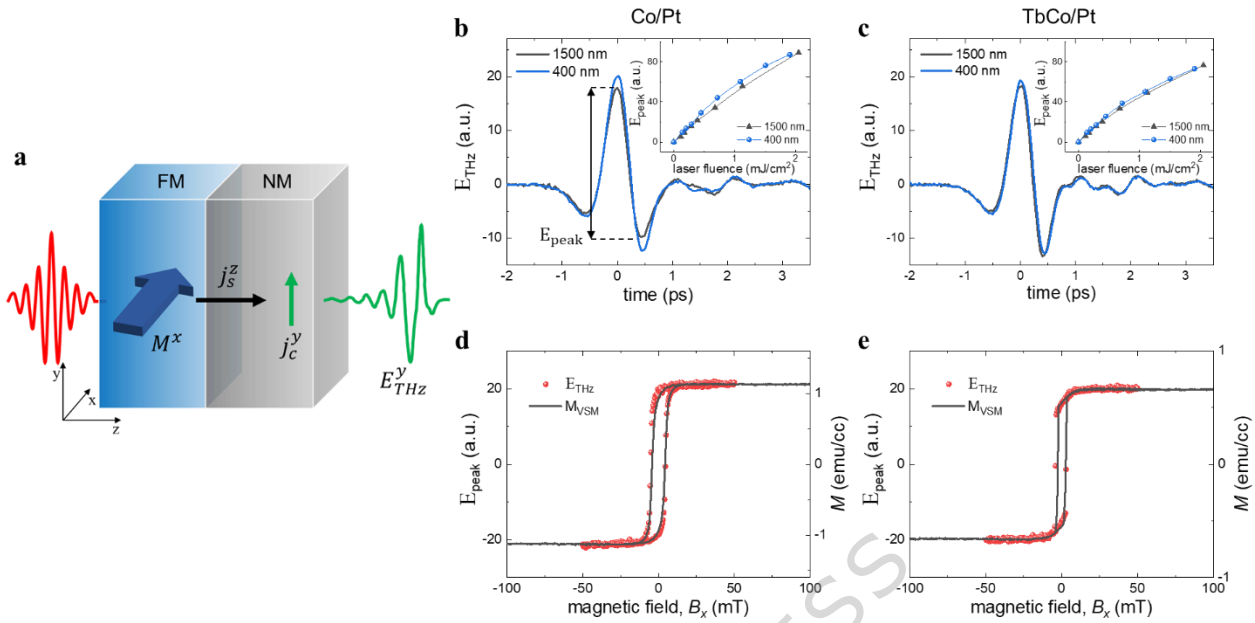

Figure 1| Single laser pulse-induced THz emission. a, Schematic diagram of THz emission via inverse spin Hall effect. **b, c,** Laser wavelength-dependent THz emission of Co/Pt and TbCo/Pt bilayers. Inset: Incident laser fluence dependence of THz amplitude. **d, e,** Comparison of magnetic hysteresis measured using 1500-nm laser-induced THz emission and with vibrating sample magnetometer (VSM) technique.

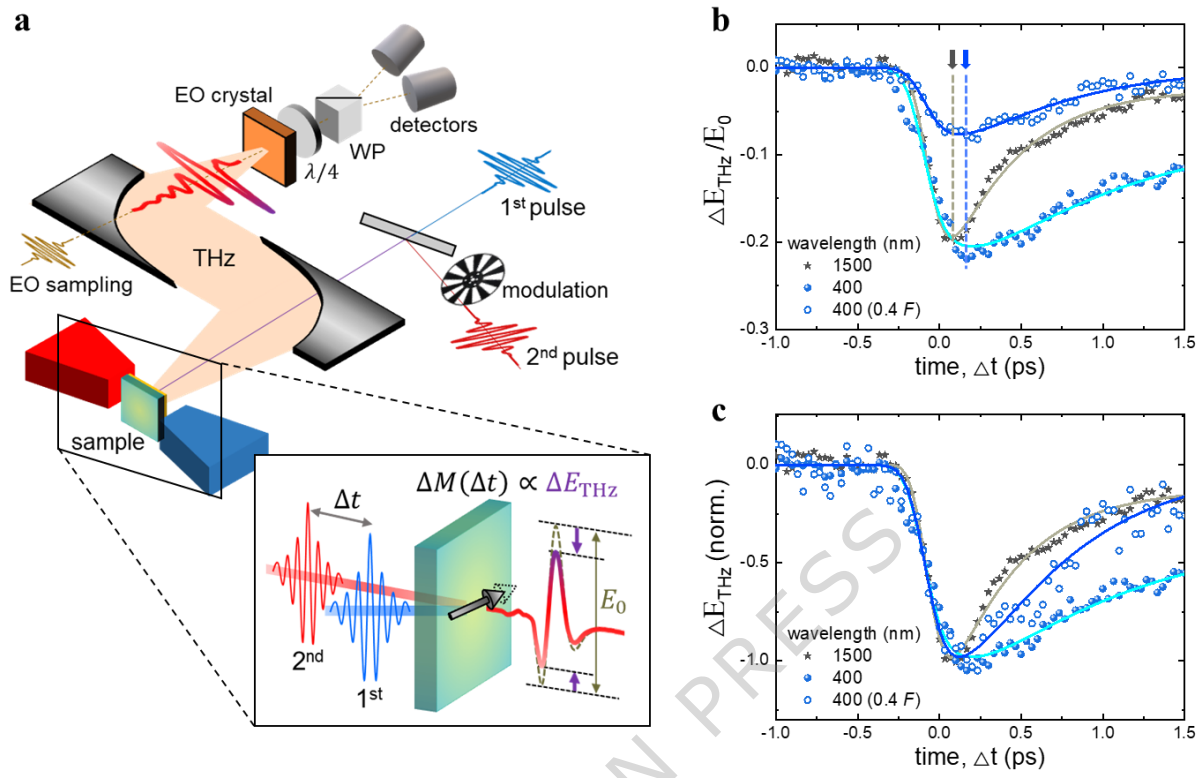

Figure 2| Double-pump THz emission spectroscopy. a, Schematic diagram of double-pump THz emission spectroscopy setup. The first pump pulse induces a magnetization change ΔM, while a second pulse detects ΔM through the change in THz field amplitude ΔE_{THz}, normalized by the THz amplitude E_0 at negative delays. **b,** ΔE_{THz} of Co/Pt bilayer induced by a 400-nm (blue, filled circle) pump pulse at an incident laser fluence of F = 800 μJ/cm^2, compared with ΔE_{THz} induced by a 1500-nm (black, star) pump pulse at a fluence (= 900 μJ/cm^2) adjusted to account for wavelength-dependent absorption, and with ΔE_{THz} induced by the 400-nm pump at a reduced fluence of 0.4F (blue, open circle). **c,** ΔE_{THz} normalized by the maximum demagnetization rate for each condition.

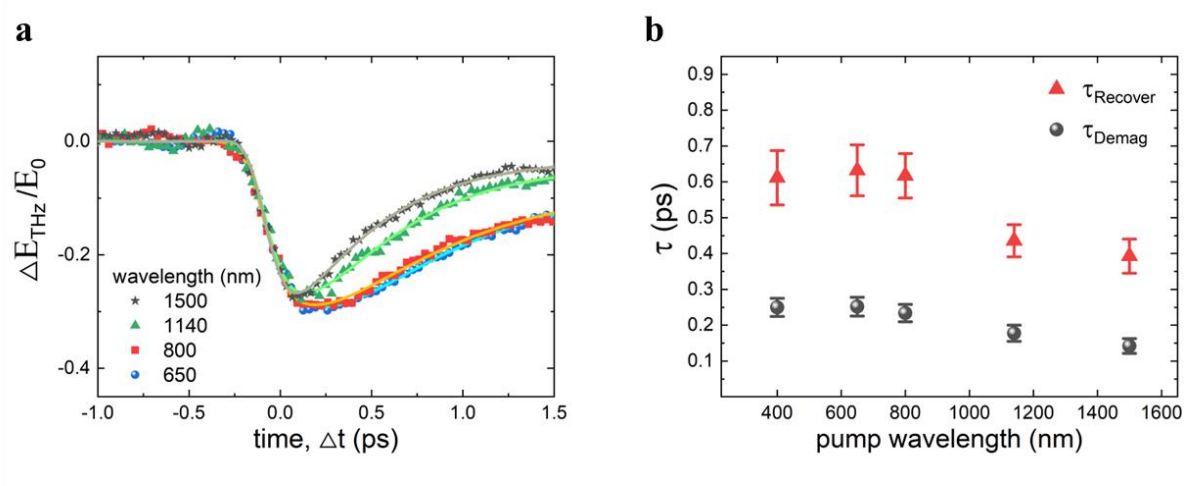

Figure 3| Wavelength-dependent magnetization dynamics of TbCo/Pt. a, ΔE_{THz} dynamics for TbCo/Pt induced by varying pump wavelengths at an incident laser fluence of F = 700 μJ/cm^2. **b,** Wavelength-dependent demagnetization and recovery times derived from **a**.

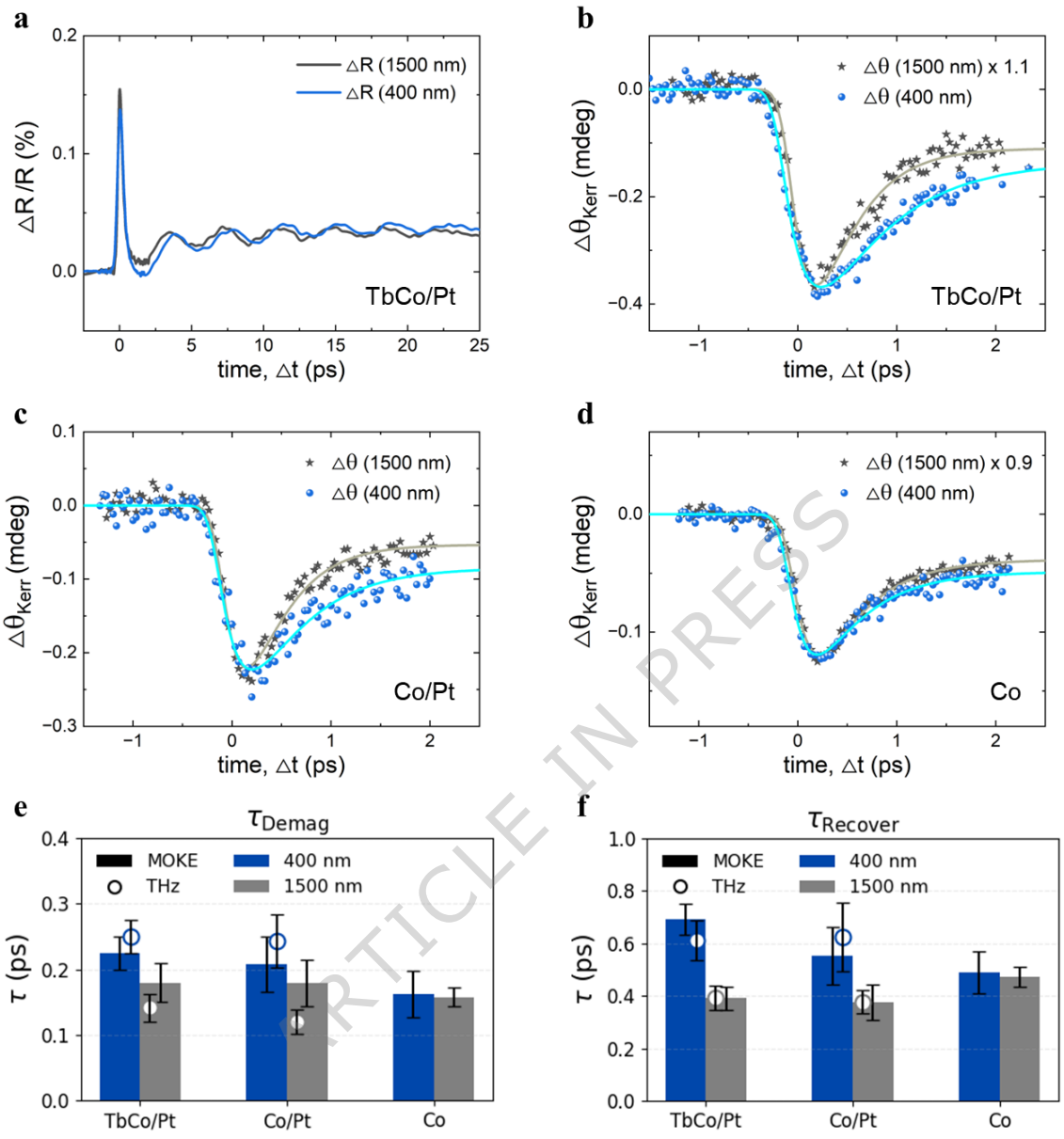

Figure 4| Time-resolved magneto-optical measurements on a single Co layer and magnetic heterostructures. a, Transient reflectance change (ΔR/R) of TbCo/Pt induced by 400-nm (900 μJ/cm^2) and 1500-nm (800 μJ/cm^2) pump pulses, measured using a linearly polarized 800-nm probe pulse. **b-d,** Magnetization-dependent Kerr rotation $\Delta\theta_{\mathrm{Kerr}}$ $[= (M_+ - M_-)/2]$ measured for (**b**) TbCo/Pt, (**c**) Co/Pt bilayers, and (**d**) a single Co layer under excitation at different pump wavelengths. **e,f,** Wavelength-dependent demagnetization and recovery times (bars) extracted from the fits in **b-d**; open circles show the corresponding time constants obtained from ΔE_{THz} (Figs. 2 and 3). Error bars represent standard errors from the fitting procedure.

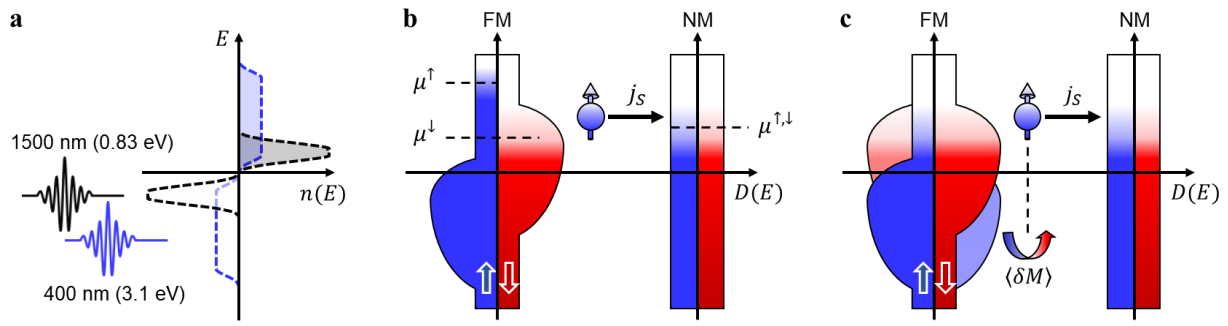

Figure 5| Influence of laser wavelength on spin transport in magnetic heterostructures. a, Pump wavelength-dependent generation of nonequilibrium electron distributions. Excitation at 1500 nm generates more localized excitations near the Fermi level compared with 400-nm excitation. **b,** Spin-dependent electron distribution creates a transient spin voltage that drives superdiffusive spin transport from the ferromagnetic (FM) to the nonmagnetic (NM) layer. **c,** Electron-magnon scattering during the relaxation of nonequilibrium distribution transfers angular momentum from magnon bath to conduction electrons, driving spin current.

Methods

1. Sample preparation

TbCo and Co films were deposited on an MgO wafer (0.5×0.25 inches) via magnetron sputtering under a base pressure of ~10^{-7} Torr. The working pressure was maintained at 3 mTorr with an Ar gas flow of 20 sccm into the chamber. The MgO layer was deposited by RF magnetron sputtering, while the TbCo and Co layers were deposited by DC magnetron co-sputtering and sputtering, respectively. The Tb sputtering power was set to 10 W, and the Co sputtering power was adjusted to 44 mW to achieve the desired TbCo composition (15:85). The M-H curves of the deposited films were measured using a vibrating sample magnetometer (VSM, LakeShore 7400).

2. THz emission spectroscopy

We used femtosecond laser pulses from a 1-kHz Ti:sapphire regenerative amplifier (Spitfire Ace, Spectra Physics) centered at 800 nm. Near-infrared laser pulses with tunable wavelengths from 1140 to 1500 nm were generated via nonlinear frequency conversion in an optical parametric amplifier (TOPAS Prime-F, Spectra Physics), which was pumped by the same regenerative amplifier. Laser pulses at 400 and 650 nm were obtained by frequency doubling of the near-infrared pulses. The pulse durations of the 800-nm fundamental and near-infrared laser pulses were measured using an autocorrelator, and remained approximately constant at ~150 fs across the tunable wavelength range. For the visible pulses, direct autocorrelation measurements were not feasible. However, the 400-nm pulses were routed through a hot mirror for collinear alignment with the near-infrared bean in the double-pump THz emission setup. This optical path likely introduced additional dispersion, and we therefore expect the 400-nm pulse to have a slightly longer duration, particularly in the double-pump configuration.

Irradiation of the sample with a single laser pulse generates a THz field via the inverse spin Hall effect (ISHE), with the polarization perpendicular to both the sample magnetization and the stacking direction of the magnetic bilayer. The generated THz fields were directed by a pair of off-axis parabolic mirrors and detected using 800-nm pulses through electro-optic sampling in a ZnTe crystal. We employed a double-pump THz emission spectroscopy scheme to monitor

magnetization depletion and spin transport. Irradiation with two high-intensity laser pulses induces a THz field generated by the first pump pulse $\boldsymbol{E_0^{1st}}$, a THz field generated by the second pump pulse $\boldsymbol{E_0^{2nd}}$, and an influence of the first pump on the THz field generated by the second pump pulse $\Delta\boldsymbol{E^{2nd}}$. Since the lock-in detection of the photoelectric signal is sensitive to the signal frequency, by modulating only the second laser pulse with a specific frequency Ω, we are able to isolate $\boldsymbol{E_0^{2nd}}(\boldsymbol{\Omega}) + \Delta\boldsymbol{E^{2nd}}(\boldsymbol{\Omega})$ from $\boldsymbol{E_0^{1st}}$. Consequently, we can measure $\Delta\boldsymbol{E^{2nd}}/\boldsymbol{E_0^{2nd}}$, which correlates with the demagnetization and spin transport processes.

3. Time-resolved reflectance and Kerr measurements

Time-resolved reflectance (ΔR/R) and magneto-optical Kerr effect ($\Delta\theta_{\mathrm{Kerr}}$) measurements were performed using a pump-probe setup based on identical laser system with THz emission spectroscopy. Pump pulses at 400 nm and 1500 nm were incident normal to the sample surface and were modulated using a mechanical chopper synchronized to the laser repetition rate to enable lock-in detection.

The probe beam, linearly polarized at 800 nm, was incident on the sample at a 20° angle. The reflected probe beam was collected and analyzed using a single photodiode detector for ΔR/R, and a Wollaston prism and balanced photodiode pair for $\Delta\theta_{\mathrm{Kerr}}$ detection. The Kerr signal, defined as $\Delta\theta_{\mathrm{Kerr}}[= (M_+ - M_-)/2]$, was extracted by reversing the in-plane magnetization direction using an external magnetic field.

References

1 Beaurepaire, E., Merle, J. C., Daunois, A. & Bigot, J. Y. Ultrafast spin dynamics in ferromagnetic nickel. *Phys Rev Lett* **76**, 4250-4253 (1996).

2 Koopmans, B., van Kampen, M., Kohlhepp, J. T. & de Jonge, W. J. M. Ultrafast magneto-optics in nickel: Magnetism or optics? *Phys Rev Lett* **85**, 844-847 (2000).

3 Koopmans, B., Ruigrok, J. J. M., Longa, F. D. & de Jonge, W. J. M. Unifying ultrafast magnetization dynamics. *Phys Rev Lett* **95**, 267207 (2005).

4 Cinchetti, M. *et al.* Spin-flip processes and ultrafast magnetization dynamics in Co: Unifying the microscopic and macroscopic view of femtosecond magnetism. *Phys Rev Lett* **97**, 177201 (2006).

5 Koopmans, B. *et al.* Explaining the paradoxical diversity of ultrafast laser-induced demagnetization. *Nat Mater* **9**, 259-265 (2010).

6 Mueller, B. Y. *et al.* Feedback Effect during Ultrafast Demagnetization Dynamics in Ferromagnets. *Phys Rev Lett* **111**, 167204 (2013).

7 Dornes, C. *et al.* The ultrafast Einstein-de Haas effect. *Nature* **565**, 209-212 (2019).

8 Tauchert, S. R. *et al.* Polarized phonons carry angular momentum in ultrafast demagnetization. *Nature* **602**, 73-77 (2022).

9 Zhang, G. P. & Hübner, W. Laser-induced ultrafast demagnetization in ferromagnetic metals. *Phys Rev Lett* **85**, 3025-3028 (2000).

10 Zhang, G. P. Laser-Induced Orbital and Spin Excitations in Ferromagnets: Insights from a Two-Level System. *Phys Rev Lett* **101**, 187203 (2008).

11 Bigot, J. Y., Vomir, M. & Beaurepaire, E. Coherent ultrafast magnetism induced by femtosecond laser pulses. *Nat Phys* **5**, 515-520 (2009).

12 Carpene, E. *et al.* Dynamics of electron-magnon interaction and ultrafast demagnetization in thin iron films. *Phys Rev B* **78**, 174422 (2008).

13 Schmidt, A. B. *et al.* Ultrafast Magnon Generation in an Fe Film on Cu(100). *Phys Rev Lett* **105**, 197401 (2010).

14 Boeglin, C. *et al.* Distinguishing the ultrafast dynamics of spin and orbital moments in solids. *Nature* **465**, 458-461 (2010).

15 Battiato, M., Carva, K. & Oppeneer, P. M. Superdiffusive Spin Transport as a Mechanism of Ultrafast Demagnetization. *Phys Rev Lett* **105**, 027203 (2010).

16 Bergeard, N. *et al.* Hot-Electron-Induced Ultrafast Demagnetization in Co/Pt Multilayers. *Phys Rev Lett* **117**, 147203 (2016).

17 Choi, G. M., Min, B. C., Lee, K. J. & Cahill, D. G. Spin current generated by thermally driven ultrafast demagnetization. *Nat Commun* **5**, 4334 (2014).

18 Bierbrauer, U. *et al.* Ultrafast magnetization dynamics in Nickel: impact of pump photon energy. *J Phys-Condens Mat* **29**, 244002 (2017).

19 Mueller, B. Y. & Rethfeld, B. Thermodynamic μT model of ultrafast magnetization dynamics. *Phys Rev B* **90**, 144420 (2014).

20 Si, M. S. & Zhang, G. P. Hot spin spots in the laser-induced demagnetization. *Aip Adv* **2**, 012158 (2012).

21 Yu. I.C., *et al.* Laser-induced coherent spin change due to spin-orbit coupling. *npj Spintronics* **3**, 4 (2025).

22 Dewhurst, J. K., Elliott, P., Shallcross, S., Gross, E. K. U. & Sharma, S. Laser-Induced Intersite Spin Transfer. *Nano Lett* **18**, 1842-1848 (2018).

23 Siegrist, F. *et al.* Light-wave dynamic control of magnetism. *Nature* **571**, 240-244 (2019).

24 Tengdin, P. *et al.* Critical behavior within 20 fs drives the out-of-equilibrium laser-induced magnetic phase transition in nickel. *Sci Adv* **4**, eaap9744 (2018).

25 Shim, J. H. *et al.* Role of non-thermal electrons in ultrafast spin dynamics of ferromagnetic multilayer. *Sci Rep* **10**, 6355 (2020).

26 Pastor, E. *et al.* Nonthermal breaking of magnetic order via photogenerated spin defects in the spin-orbit coupled insulator Sr3Ir2O7. *Phys Rev B* **105**, 064409 (2022).

27 Chekhov, A. L. *et al.* Ultrafast Demagnetization of Iron Induced by Optical versus Terahertz Pulses. *Phys Rev X* **11**, 041055 (2021).

28 Stiehl, M. *et al.* Role of primary and secondary processes in the ultrafast spin dynamics of nickel. *Appl Phys Lett* **120**, 062410 (2022).

29 Cardin, V. *et al.* Wavelength scaling of ultrafast demagnetization in Co/Pt multilayers. *Phys Rev B* **101**, 054430 (2020).
30 Seibel, C. *et al.* Control of transport phenomena in magnetic heterostructures by wavelength modulation. *Phys Rev B* **106**, L140405 (2022).
31 Kampfrath, T. *et al.* Terahertz spin current pulses controlled by magnetic heterostructures. *Nat Nanotechnol* **8**, 256-260 (2013).
32 Rouzegar, R. *et al.* Laser-induced terahertz spin transport in magnetic nanostructures arises from the same force as ultrafast demagnetization. *Phys Rev B* **106**, 144427 (2022).
33 Saitoh, E., Ueda, M., Miyajima, H. & Tatara, G. Conversion of spin current into charge current at room temperature: Inverse spin-Hall effect. *Appl Phys Lett* **88**, 182509 (2006).
34 Valenzuela, S. O. & Tinkham, M. Direct electronic measurement of the spin Hall effect. *Nature* **442**, 176-179 (2006).
35 Seifert, T. *et al.* Efficient metallic spintronic emitters of ultrabroadband terahertz radiation. *Nat Photonics* **10**, 483-488 (2016).
36 Wang, Z. Q., Ren, W. J., Zhang, G. Y. & Wang, Z. Y. Characterization of the Stress-optic Properties of Ceramics by Terahertz Time-domain Spectroscopy. *Curr Opt Photonics* **8**, 225-229 (2024).
37 Battiato, M., Carva, K. & Oppeneer, P. M. Theory of laser-induced ultrafast superdiffusive spin transport in layered heterostructures. *Phys Rev B* **86**, 024404 (2012).
38 Bauer, G. E. W., Saitoh, E. & van Wees, B. J. Spin caloritronics. *Nat Mater* **11**, 391-399 (2012).
39 Alekhin, A. *et al.* Femtosecond Spin Current Pulses Generated by the Nonthermal Spin-Dependent Seebeck Effect and Interacting with Ferromagnets in Spin Valves. *Phys Rev Lett* **119**, 017202 (2017).
40 Légaré, K. *et al.* Near- and mid-infrared excitation of ultrafast demagnetization in a cobalt multilayer system. *Phys Rev B* **109**, 094407 (2024).
41 Li, G. *et al.* Ultrafast kinetics of the antiferromagnetic-ferromagnetic phase transition in FeRh. *Nat Commun* **13**, 2998 (2022).
42 Saito, Y., Kholid, F. N., Karashtin, E., Pashenkin, I. & Mikhaylovskiy, R. V. Terahertz Emission Spectroscopy of Exchange-Biased Spintronic Heterostructures: Single- and Double-Pump Techniques. *Phys Rev Appl* **19**, 064040 (2023).
43 Wang, B. *et al.* Picosecond nonlinear spintronic dynamics investigated by terahertz emission spectroscopy. *Appl Phys Lett* **115**, 121104 (2019).
44 F. Dalla Longa et al. Influence of photon angular momentum on ultrafast demagnetization in nickel, *Phys. Rev. B* **75**, 224431 (2007).45 Eesley, G. L. Generation of Nonequilibrium Electron and Lattice Temperatures in Copper by Picosecond Laser-Pulses. *Phys Rev B* **33**, 2144-2151 (1986).
46 Sun, C. K., Vallee, F., Acioli, L. H., Ippen, E. P. & Fujimoto, J. G. Femtosecond-Tunable Measurement of Electron Thermalization in Gold. *Phys Rev B* **50**, 15337 (1994).
47 Carpene, E. Ultrafast laser irradiation of metals: Beyond the two-temperature model. *Phys Rev B* **74**, 024301 (2006).
48 Kimling, J. & Cahill, D. G. Spin diffusion induced by pulsed-laser heating and the role of spin heat accumulation. *Phys Rev B* **95**, 014402 (2017).
49 Beens, M., Duine, R. A. & Koopmans, B. Modeling ultrafast demagnetization and spin transport: The interplay of spin-polarized electrons and thermal magnons. *Phys Rev B* **105**, 144420 (2022).
50 Kang, K. *et al.* Spin current driven by ultrafast magnetization of FeRh. *Nat Commun* **14**, 3619 (2023).
51 Caminale, M. *et al.* Spin pumping damping and magnetic proximity effect in Pd and Pt spin-sink layers. *Phys. Rev. B* **94**, 014414 (2016).
52 Eich, S. *et al.* Band structure evolution during the ultrafast ferromagnetic-paramagnetic phase transition in cobalt. *Sci. Adv.* **3**, e1602094 (2017).
53 Johnson P. B. & Christy R. W. Optical constants of transition metals: Ti, V, Cr, Mn, Fe, Co, Ni, and Pd. *Phys. Rev. B* **9**, 5056 (1974).

Acknowledgements

This work was supported by the National Research Foundation of Korea (NRF) funded by the Korean Government (MSIP) (grant numbers: RS-2023-00208484, RS-2024-00408271, RS-2023-00275259, RS-2023-00207732) and the Korea Institute of Energy Technology Evaluation and Planning (KETEP) (20224B10100040).

Author contributions

I.C.Y. and S.K. conducted the research under the supervision of K.-J.K. and F.R. I.C.Y. performed the THz measurements with the help of W.T.K and B.S.H. and data analysis. S.K. prepared the samples with the help of B.K.P. and carried out the VSM measurements. I.C.Y, S.K., K.-J.K, and F.R. wrote the manuscript. All authors are involved in the discussion of the results and commented on the manuscript.

Competing interests

The authors declare that they have no competing interests.

Data Availability

The data supporting the findings of this study are available from K.-J.K. and F.R. upon reasonable request.

ED summary:

Laser-induced ultrafast demagnetization has been thought to depend mainly on total absorbed laser power, with little regard for photon energy. Here, the authors use spintronic terahertz emission spectroscopy to demonstrate that photon energy significantly influences magnetization dynamics, revealing that shorter-wavelength high-energy photons extend demagnetization and recovery time scales, thus providing interesting insights and opportunities for optical control in spintronics.

Peer review information:

Communications Materials thanks the anonymous reviewers for their contribution to the peer review of this work. A peer review file is available.